Pennate actuators: Force, contraction, and stiffness

To cite this article before publication: Tyler E Jenkins *et al* 2020 *Bioinspir. Biomim.* in press https://doi.org/10.1088/1748-3190/ab860f

Pennate Actuators: Force, Contraction, and Stiffness

Tyler Jenkins and Matthew Bryant
North Carolina State University, Department of Mechanical and Aerospace Engineering

Abstract

Hierarchical actuators are comprised of multiple individual actuator elements arranged into a system, resulting in improved and expanded performance. Natural muscle tissue is a complex and multi-level example of hierarchical actuation, with its hierarchy spanning from the micrometer to the centimeter scale. In addition to a hierarchical configuration, muscle tissue exists in varying geometric arrangements. Pennate muscle tissue, denoted by its characteristic fibers extending obliquely away from the muscle tissue line of action, leverages geometric complexity to transform the relationship between fiber inputs and muscle tissue outputs. In this paper, a bioinspired hierarchical pennate actuator is detailed. This work expands on previous pennate actuator studies by deriving constitutive force, contraction, and stiffness models for a general pennate actuator, where the constituent fibers can be constructed from any linear actuator. These models are experimentally validated by studying a pennate actuator with McKibben artificial muscles constituting the actuator fibers. McKibben artificial muscles are used because they have a high force-to-weight ratio and are inexpensive to construct, making them an attractive candidate for hierarchical actuators and mobile robotics. Using the derived constitutive models, general pennate actuator performance is better understood by analyzing the transmission ratio, blocked force, and free contraction. Loaded contractions and stiffness during isotonic and isobaric contractions are also explored. The results allow for informed design decisions and an understanding of the associated tradeoffs when recreating the remarkable properties of pennate musculature. Future work will leverage the results of this paper to create an adaptive pennate actuator that is capable of changing configuration in response to force, contraction, and stiffness demands.

Introduction

Hierarchical actuators incorporate multiple individual actuators into geometrically complex macro-level systems to enable advantageous functionality. By integrating multiple actuators into a hierarchical configuration, the resulting speed, force, efficiency, stroke, and redundancy can be tailored. This approach has proven useful in cellular piezoelectric actuators [1], whiffletree actuators [2], series-parallel approaches [3], and bio-inspired actuator recruitment [4], which utilize multiple small actuators to expand actuator bandwidth and efficiency. Because current mobile robotics applications need energetic improvements [5], hierarchical actuation schemes are of research interest. When considering hierarchical actuation schemes in nature, biological muscle tissue offers a dramatic example. A muscle tissue's hierarchy is organized into sequentially larger groups progressing from sarcomeres (where the contractile protein interactions take place) at the smallest level, to myofibrils, fibers, fascicles, and finally entire muscles at the largest level. Recent studies have used muscle-inspired hierarchies to create bundles of linear actuators that mimic biological orderly recruitment schemes to improve efficiency [4]. Similar to mammalian muscles, by purposely using a bundle's smallest necessary motor unit, the energy consumed is minimized. Actuator bundles currently configure the individual actuators in parallel – i.e., the

longitudinal axis of each linear actuator is oriented in the same direction as the overall actuator line-of-action [6]. However, in nature many muscle topologies exist that deviate from this parallel arrangement; this paper considers a pennate arrangement.

In contrast to their parallel-fibered counterpart, pennate muscle tissue has fibers oriented at an oblique angle relative to the muscle tissue's contractile line-of-action [7]. Pennate muscle tissues have demonstrated unique properties; in a series of papers outlining the biological advantages of pennate musculature [8–10], the implications of the muscle fibers' oblique orientation on fast contractions, shock absorption, aging, and damage prevention during extension were explored. Furthermore, pennate muscle tissue was shown to passively regulate its thickness and bulging, altering the effective gear ratio coupling the fiber force and displacement to the macro-level muscle force and displacement [8]. These effects are attributed to pennate muscles effectively functioning with a variable gear ratio, where the gearing dictates the relationship between fiber inputs and muscle outputs. Presently, the literature exploring bio-mimetic pennate actuators is sparse. In 2013, a uni-pennate actuator implementing McKibben artificial muscle actuators was outlined [11]. The authors showed that the variable gearing concept exists in a uni-pennate array prototype. In 2014, variable stiffness and recruitment using nylon actuators in a pennate topology was explored experimentally [12]. Although both studies provide a promising baseline, a constitutive model relating the "fiber" actuator force, position, and stiffness to the "muscle" actuator force, position, and stiffness has not been developed.

Beyond readily integrating with other bio-inspired hierarchical actuator technologies, such as orderly recruitment, understanding the constitutive relationships will allow the development of a pennate actuator as a Variable Stiffness Actuator (VSA). VSA's are useful for roboticists and engineers because they enable features atypical of traditional, stiff kinematic linkages, such as energy storage or increased human-interaction safety. Traditionally, robots are designed with minimal compliance to enable precise trajectory tracking and high bandwidth. However, by intentionally introducing compliance into the drivetrain of a robot, advantages such as shock tolerance, low reflected inertia, stable force control, decreased damage during contact, and potential for energy storage are possible [13]. By adaptively varying the actuator stiffness, VSA's can improve actuator performance by adjusting stiffness to the task at hand [14,15]. If human interactive safety is of concern, optimal control theory has been used to determine upper bounds on actuator stiffness, thus reducing the engineering tradeoff on tracking performance, all while quantitatively remaining safe [16].

This paper explores the modeling, design, experimental validation, and analysis of a bio-inspired pennate hierarchical actuator. The development of analytic models allows for a deeper understanding of the coupling between force, stiffness, and speed of the individual "fibers" and the net "muscle" output. To this end, first the muscle-level force and strain are related to the fiber-level force and strain via a constitutive kinematic model, resulting in a relationship for the transmission ratio and an actuator stiffness model. Next, a hardware proof-of-concept is built to validate the stiffness model. A pennate hierarchical actuator is then constructed from McKibben pneumatic actuators. Existing McKibben actuator analytic models are modified for use with the newly developed pennate relationships, and experimental data is collected on a custom actuator testing machine. Finally, the models are used to analyze specific cases, providing further insight into actuator characteristics.

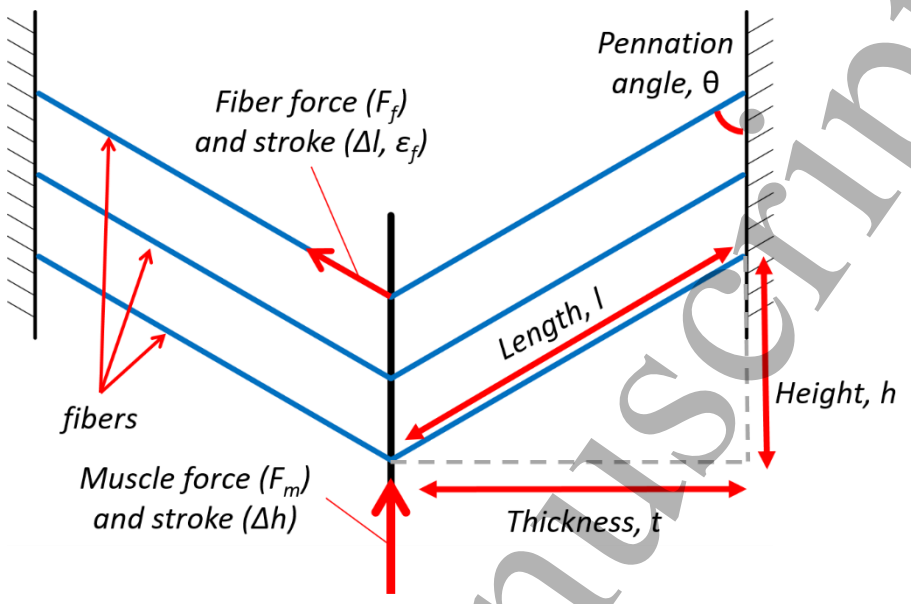

Figure 1: A diagram of the pennate topology. "Fibers" are arranged obliquely to the "muscle" line of action via a pennation angle. The muscle is made up of multiple individual fibers.

Kinematic model and gear ratio

In mammalian musculature, pennate muscle tissue is denoted by muscle fibers extending obliquely away from a central connective tissue. This pattern has the appearance of a feather, hence the Latin *penna*, meaning feather. Due to the muscle fibers' oblique orientation, the muscle fiber forces generated are not entirely directed along the tissue's line of action, thus attenuating the force transmission. During a contraction, the muscle fibers rotate, altering the force component oriented along the line of action. Fiber rotation amplifies the fiber contraction, meaning the pennate muscle tissue has a greater contraction than that of an individual fiber. Pennate muscle configuration effectively functions as a variable transmission ratio, capable of passively arranging into a favorable configuration for the demanded actuation task. Connective tissue is thought to passively regulate the fiber rotation [8]. During a contraction, the material properties of a highly loaded pennate muscle tissue allow the muscle fibers to orient more parallel to the line of action (reducing pennation angle and favoring force output), whereas a minimally loaded pennate muscle tissue's fibers are more obliquely oriented to the line of action (increasing pennation angle and favoring velocity output)[8]. Thus, pennate muscle tissue passively adapts to a favorable configuration based on the load. When considering a pennate actuator in lieu of biological tissue, individual linear actuators are analogous to muscle fibers, whereas the entire pennate configuration is analogous to a whole muscle tissue. The fiber (i.e. individual actuator) force, strain, and activation are the inputs, and the muscle tissue (i.e. bulk pennate actuator) force and strain are the outputs.

To understand the actuator-agnostic force and geometric amplification of the pennate configuration, the kinematic relationships governing force attenuation and stroke amplification are explored in this section. Of interest are the relationships of muscle force to fiber force, muscle stroke to fiber stroke, muscle and fiber stroke to changing pennation angle, and fiber stiffness to muscle stiffness. Kinematics are used to relate the muscle and fiber through the formulation of a *transmission ratio*. This is analogous to the architectural gear ratio (AGR) shown in biomechanics studies [8]. Throughout this paper, the term *fiber*

refers to an individual actuator and fiber parameters are denoted with a subscript *f*, while the term *muscle* refers to the bulk actuator with parameters denoted by a subscript *m*.

Transmission ratio

A pennate actuator diagram is shown in Figure 1 and is used to relate the muscle force F_m to the fiber force F_f in equation (1), where *n* is the number of fibers, and θ is the pennation angle.

$$F_m = F_f n \cos\theta \tag{1}$$

Functional biomechanics models and schematics similar to that in Figure 1 have been dated as far back as 1664 [17], and have been of continuing interest to biomechanics researchers [18,19]. Using equation (1), the transmission ratio relating output muscle force to input fiber force is

$$TR_{force} = \frac{F_m}{nF_f} = \cos\theta \tag{2}$$

where TR_{force} is the transmission ratio relating the output force to input force. Assuming constant thickness, the transmission ratio relating the contraction rates of the fiber and muscle is

$$TR_{position} = \frac{dh}{dl} = \frac{d}{dl}\left(\sqrt{l^2 - t^2}\right) = \frac{l}{\sqrt{l^2 - t^2}} = \frac{l}{h} = \sec\theta \tag{3}$$

where $TR_{position}$ is the transmission ratio relating a differential change in muscle output length to a differential change in fiber input length. Note that TR_{force} and $TR_{position}$ are reciprocals, as expected. By understanding the transmission ratio, the pennate actuator is classified as operating via a "continuously variable transmission" mechanism, one of the many high-level variable stiffness actuator (VSA) groups outlined in the comprehensive VSA review papers [14,20]. The transmission ratio is later used to analyze the relationship between pennate muscle outputs, fiber actuator contraction, and initial position.

General Stiffness Model

The pennate muscle stiffness, k_m, is defined as the ratio of a differential change in muscle force to a differential change in muscle position. A stiffer actuator will exert a greater force in response to a unit displacement as compared to a less stiff actuator. Differentiating equation (1) with respect to the output position, and noting that $\cos\theta = h/l$, pennate muscle stiffness is

$$k_m = \frac{dF_m}{dh} = n\left[\frac{dF_f}{dh}\frac{h}{l} + \frac{F_f}{l}\frac{dh}{dh} + F_f h \frac{d}{dh}\left(\frac{1}{l}\right)\right], \tag{4}$$

and via the chain rule:

$$k_m = n\left[\frac{dF_f}{dS_f}\frac{dS_f}{dl}\frac{dl}{dh}\frac{h}{l} + \frac{F_f}{l} + F_f h \frac{d}{dl}\left(\frac{1}{l}\right)\frac{dl}{dh}\right] \tag{5}$$

where the extending fiber strain S_f is

$$S_f = \frac{l - l_0}{l_0} \tag{6}$$

and the necessary derivatives are

$$\frac{dS_f}{dl} = \frac{1}{l_0} \tag{7}$$

$$\frac{dl}{dh} = \frac{h}{\sqrt{h^2 + t^2}} = \frac{h}{l} \tag{8}$$

$$\frac{d}{dl}\left(\frac{1}{l}\right) = -\frac{1}{l^2} \ . \tag{9}$$

Substituting and simplifying yields:

$$\begin{aligned} k_m &= n\left[\frac{dF_f}{dS_f}\frac{h^2}{l^2 l_0} + F_f\frac{l^2 - h^2}{l^3}\right] = n\left[\frac{dF_f}{dS_f}\frac{l^2 - t^2}{l^2 l_0} + F_f\frac{t^2}{l^3}\right] \\ &= n\left[\frac{dF_f}{dS_f}\frac{1}{l_0}\left(1 - \frac{t^2}{l^2}\right) + F_f\frac{t^2}{l^3}\right] \end{aligned} \ . \tag{10}$$

Recognizing that $\frac{t^2}{l^2} = \sin^2\theta$ and $1 - \sin^2\theta = \cos^2\theta$, we arrive at:

$$k_m = \frac{n}{l_0}\left[\frac{dF_f}{dS_f}\cos^2\theta + \frac{F_f}{1 + S_f}\sin^2\theta\right] \ . \tag{11}$$

Equation (11) is general for any actuator "fiber" in a pennate "muscle" configuration. It relates the fiber force, initial actuator configuration, current actuator configuration, and fiber stiffness to compute the muscle stiffness.

Stiffness model validation

As a proof of concept, a simple pennate device is constructed for experimental validation of the stiffness model. The setup, shown in Figure 2a, is made of 3D printed components connected by linear springs in a pennate configuration. The outer connection points are movable to discretely adjust the thickness of the pennate device. Force vs position data are collected by slowly changing the "muscle" position and recording the "muscle" force. Control and data collection were executed by a National Instruments cRIO FPGA/Real-Time Controller with a custom actuator testing machine. Actuator position was controlled in open-loop via a non-back-drivable stepper motor and lead screw with a resolution of 0.0025 cm/step, driven in 1/16 step-per-pulse mode to minimize vibration. Actuator force was measured using a six-axis ATI Gamma load cell with a maximum z-axis force of 200 N and a resolution of 0.025 N. All testing was performed at a slow contraction rate of 0.1 mm/s to approximate a quasi-static condition.

The force vs position data are first collected for individual linear springs in a parallel configuration to validate the manufacturer spring constant and verify a linear force-position relationship. Appropriate end fittings are used to ensure the spring remained collinear with the stroke of the linear actuator. The individual spring constant is used as an input parameter to the pennate analytic models given in equations (1) and (11). Next, quasi-static force vs position data are collected for linear springs in a pennate configuration. Five trials are conducted at a thickness of 3.2 cm. Data is collected at 1 kHz and low-pass filtered in software. The force vs displacement curve in Figure 2 is obtained by computing the mean and standard deviation of the five trials, with data points and error bars (representing one standard deviation) displayed at 0.5 cm intervals. Stiffness is computed by fitting the force vs position data via a Savitzky-Golay filter [21], creating a smooth fit with a differentiable function. Each trial is fit and differentiated in this manner. The data is then plotted against the linear spring pennate model, shown in Figure 2a. The force data shows good agreement with the model. Experimental errors are attributed to the friction between the sliding 3D printed components. The two small bumps in Figure 2c near 7 and 9 cm are due to the springs beginning to contact one another; note that, because stiffness is the derivative of the force vs strain curve, subtle changes in the force measurement lead to shape changes in the stiffness vs position curve. The stiffness, shown in Figure 2c, follows the correct trend of the model, however oscillating peaks are present in the differentiated data. These are the result of small changes in the force vs stroke curve that manifest as roughness in the derivative. Interestingly, the pennate configuration has a non-constant stiffness, even though the actuators have a constant stiffness. This behavior is due to the nonlinear relationship between the “fiber” force, stroke, and stiffness and the “muscle” force, stroke, and stiffness,

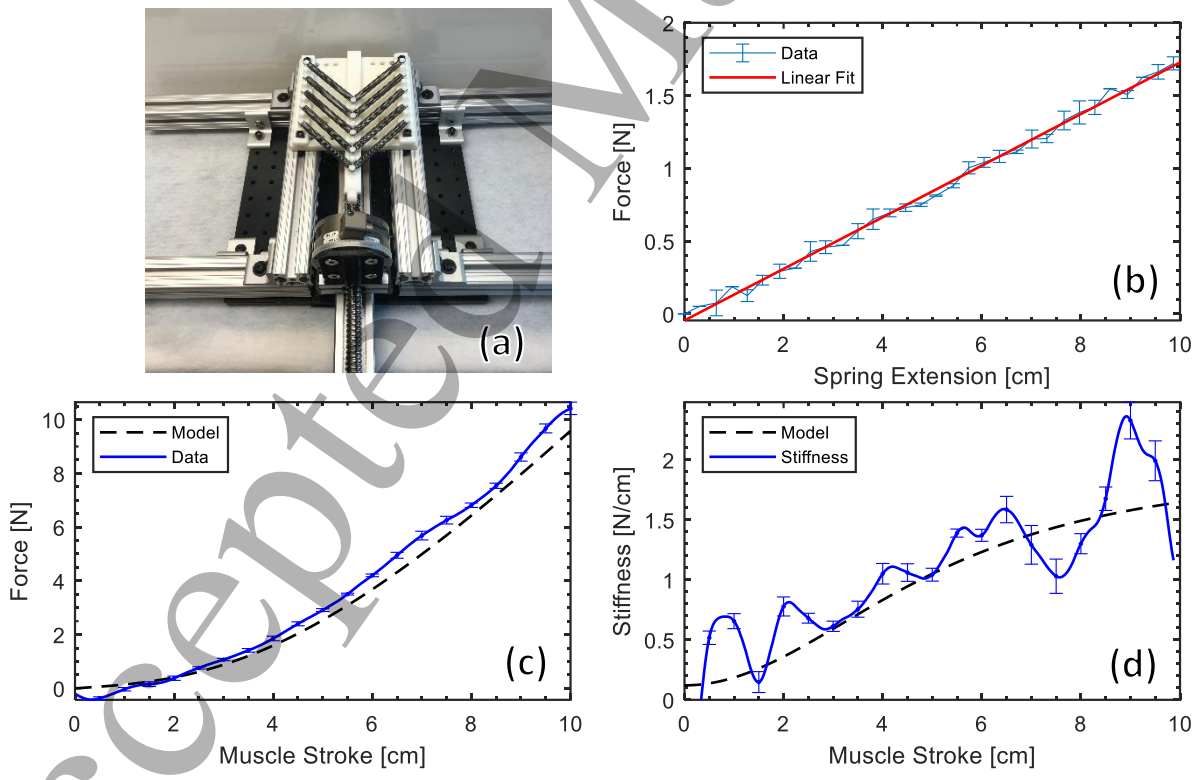

Figure 2: (a) Ten constant stiffness linear springs are arranged in a pennate configuration with adjustable thickness, (b) Force vs position data for a single linear spring, (c) Pennate force vs position data, (d) Pennate stiffness vs position data. Stiffness is analytically computed via the general stiffness model and compared with the derivative of the measured data.

as shown in equation (11). As the pennate muscle length changes, the linear springs rotate, changing the configuration and force transmission, leading to this nonlinear relationship. Additionally, note that the stiffness model gives non-zero stiffness at zero stroke. For this configuration, the springs had a slight stretch at a 90 degree pennation angle, therefore leading to the second term of equation (11) having a non-zero value.

McKibben Actuator Experiments – data, modeling, and validation

McKibben actuators (often called McKibben muscles or fluidic artificial muscles) are lightweight, easy to construct, and naturally compliant linear actuators. They are generally constructed using an elastomeric inner tube surrounded by a braided sheath, shown in Figure 3. A pressurized working fluid is applied through one end of the actuator, resulting in radial expansion and axial contraction. Because of their high force-to-weight ratio, McKibben actuators can be assembled into bundles [22,23]; for these reasons, they are an ideal actuator candidate for a bio-inspired hierarchical pennate actuator. To develop the McKibben pennate actuator concept in this section, first an individual McKibben actuator is modeled (i.e., the "fiber model"). The fiber model is then validated using quasi-static experimental data. Next, the fibers are assembled into a pennate muscle. Using the models developed earlier, a McKibben pennate muscle model is derived. The model is then validated using quasi-static experimental data.

The data collection system used the same cRIO, load cell, and lead screw as in the previous section. In addition, closed-loop pressure control is added to maintain pressure in the McKibben actuators during testing, as shown in Figure 4. The system controls actuator pressure in closed-loop using a pneumatic 5/3-Servo Valve (MPYE, Festo). Pressure feedback is measured with an analog pneumatic pressure transducer rated to 689 kPa (100 PSI, Measurement Specialties, Inc.), and is conditioned with an instrumentation amplifier circuit. PID pressure control is executed at 1 kHz. Before quasi-static data is collected for the entire pennate muscle actuator, data is first collected for a single McKibben fiber to facilitate the computation of blocked-force and free-strain correction factors, as defined in the next section.

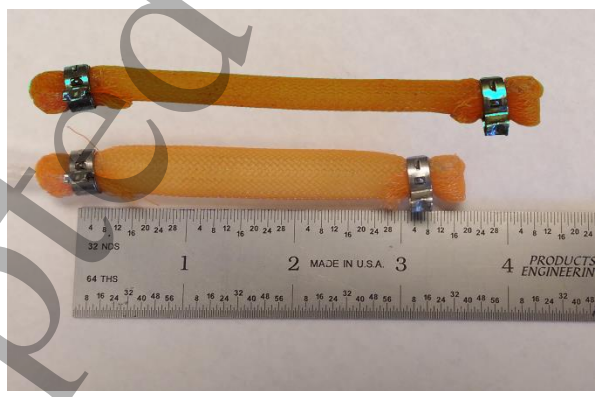

Figure 3: An example of an unpressurized (top) and pressurized (bottom) pneumatic McKibben actuator

McKibben actuator – pennate actuator fiber model

McKibben actuators embody the fibers of the pennate actuator. To better understand the performance of the McKibben pennate actuator, the McKibben fiber is modeled using virtual work principles [24], resulting in an ideal force-strain McKibben model, shown in equation (12),

$$F_{f,ideal} = P\pi r_0^2 \left(a\left(1-\varepsilon\right)^2 - b \right) \tag{12}$$

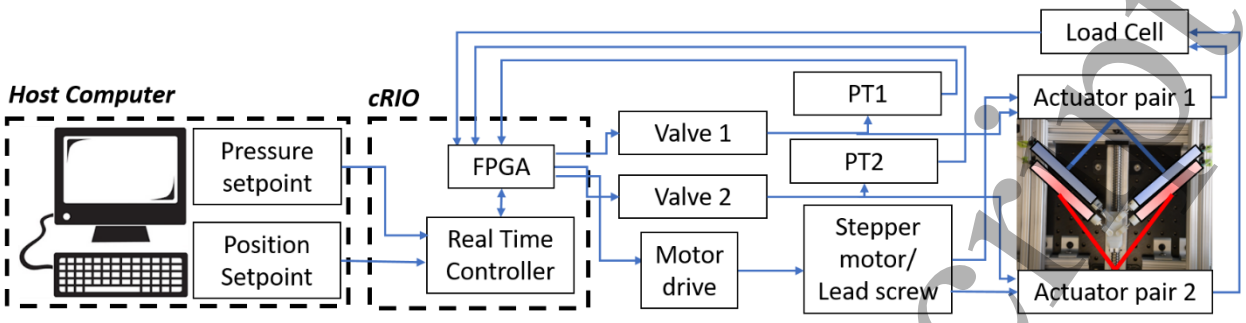

Figure 4: System block diagram for the actuator test stand. The system uses a LabVIEW host program, communicating with a NI cRIO FPGA/Real-Time Controller. cRIO inputs are load cell signals and pressure transducer (PT) signals amplified by an instrumentation amplifier circuit. Outputs are servo valve position signals and a motor drive signal.

$$a = \frac{3}{\tan^2 \alpha_0}, \quad b = \frac{1}{\sin^2 \alpha_0} \tag{13}$$

$$\varepsilon = \frac{l_0 - l}{l_0} = -S_f \tag{14}$$

where P is the applied pressure, r_0 is the initial bladder radius, a and b are constants determined by the initial braid angle relative to the longitudinal axis, α_0 is the initial braid angle with respect to the longitudinal axis, and ε is the contractile strain. Note that, while strain is generally defined as in equation (6), the notation ε and its definition are used in this section to remain consistent with the McKibben actuator literature.

In practice, the McKibben ideal force-strain model is accurate for high pressures and for McKibben actuators constructed with inner bladders of negligible stiffness. However, the model requires correction factors when considering ordinary elastic bladder materials, such as commonplace latex. To this end, correction factors have been developed to adjust the axis zero-intercepts of the force-strain curves [24,25]. The corrected virtual work model is used because it provides a balanced tradeoff between the simplicity of the virtual work model, while still capturing many of the complexities introduced by elastic effects. A systematic method for determining these correction factors was later developed [26] and is used here. The modified McKibben actuator force is modeled as

$$F_{f,mod} = \kappa_F P \pi r_0^2 \left(a\left(1 - \kappa_\varepsilon \varepsilon\right)^2 - b \right) \tag{15}$$

where κ_F is the blocked-force correction factor and κ_ε is the free-strain correction factor. Both correction factors are functions of pressure and are determined by curve-fitting empirical data. At the blocked-force condition, strain is equal to zero and a McKibben actuator's force is maximized for a given pressure. Solving equation (15) for the blocked-force correction factor yields

$$\kappa_F = \frac{F_{f,blocked}(P)}{P \pi r_0^2 (a - b)} \tag{16}$$

where $F_{f,blocked}(P)$ is a polynomial as a function of pressure, determined via curve fit to experimentally measured blocked-force data. At the free-strain condition, force is equal to zero and a McKibben actuator's contraction is maximized for a given pressure. Similarly, the free-strain correction factor is solved in equation (15) at the zero force condition, giving

$$\kappa_\varepsilon = \frac{1}{\varepsilon_{free}(P)}\left(1-\sqrt{\frac{b}{a}}\right) \tag{17}$$

where $\varepsilon_{free}(P)$ is a polynomial as a function of pressure, determined via curve fit to experimentally measured free-strain data points. The fiber stiffness is then derived as

$$k_f = \frac{2\kappa_\varepsilon \kappa_F \pi r_0^{\,2} Pa}{l_0}\left(1-\kappa_\varepsilon \varepsilon\right) . \tag{18}$$

Table 1: McKibben actuator fiber initial parameters.

Parameter	Value
r_0	0.25 [cm]
α_0	20.8°
l_0	13.56 [cm]

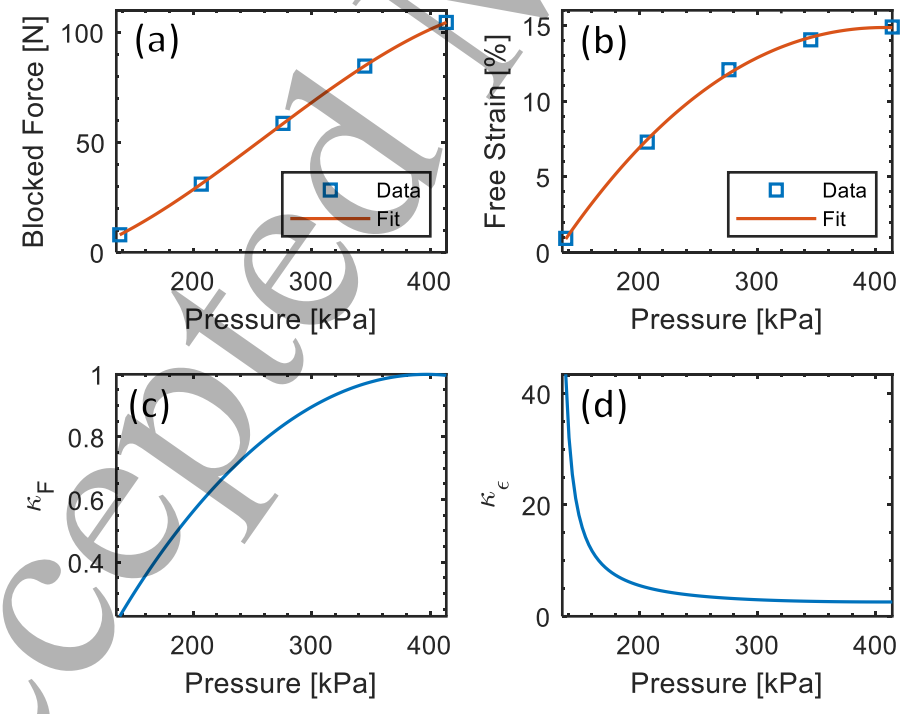

Figure 5: (a) Experimental blocked-force and (b) free-strain data as a function of pressure is collected and used to compute the (c) blocked-force correction factor and the (d) free-strain correction factor. Correction factors approach unity as pressure increases.

Using the actuator testing machine described previously, the blocked-force and free-strain as functions of pressure are measured and plotted in Figure 5. Note that because the above models deal with a single McKibben fiber, only one actuator is tested at a time and it is oriented collinear with the lead screw. Curves are fit to the blocked-force and free-strain data, with the resulting equations and coefficients shown in equation (19) and Table 2. For equation (19), *f(P)* represents either the blocked-force correction factor or the free-strain correction factor, contingent upon which set of coefficients are used from Table 2. Equation (19)'s input pressure is in Pascals, and the outputs are Newtons (for the blocked-force correction factor) and decimal strain contraction (for the free-strain correction factor). Data is not presented at low pressures because the McKibben fiber does not begin contracting until ~138 kPa is applied, due to the bladder elasticity and braid material properties [27]. Both correction factors are fit with a third order polynomial, with coefficients described in equation (19) and Table 2. The curve fit is valid from 138 kPa to 550 kPa (20 to 60 PSI).

$$f(P) = c_1 P^3 + c_2 P^2 + c_3 P + c_4, \quad 138000 \le P \le 550000 \quad [\text{Pa}] \tag{19}$$

Table 2: Coefficients for the blocked-force and free-strain curve fit.

Coefficient	Blocked Force [N]	Free Strain
c_1	-2.715e-15	1.188e-18
c_2	2.127e-09	-3.063e-12
c_3	-1.522e-4	1.903e-06
c_4	-4.387	-0.1984

The blocked-force and free-strain correction factors are then used to compute the modified McKibben model using equations (15)-(17) and (19). Quasi-static contraction data is collected for pressures of 207 kPa (30 PSI) and 276 kPa (40 PSI), and is plotted against the fiber model in Figure 6a. The force model shows good agreement with the data. Note that the slope of the force-strain model slightly differs from the experiment, which is attributed to braid friction and material effects that are not entirely accounted for by the correction factors. The single McKibben stiffness is shown in Figure 6b. Stiffness is again computed using the Savitzky-Golay filter approach. Any McKibben model parameter uncertainty, or unmodeled effects such as hysteresis and friction, will lead to the model deviating from the measured data. This effect, in turn, causes the stiffness model to deviate from the computed data. The average

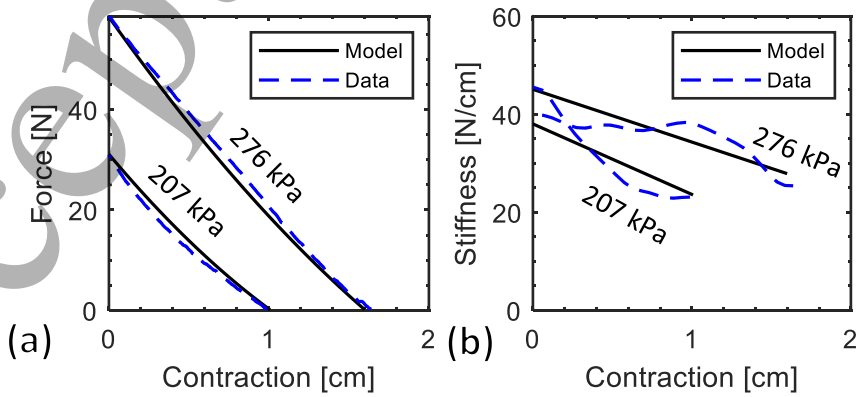

Figure 6: (a) Quasi-static force-contraction and (b) stiffness-contraction data and model for a single McKibben actuator

experimental percent error for the 207 kPa stiffness case is 10.6%, and is 7.7% for the 276 kPa stiffness case.

McKibben actuator pennate muscle model

The McKibben fiber model is next implemented in the pennate muscle model. The additional length of the end fittings is accounted for by distinguishing between the McKibben actuator length, l, and the entire fiber length, l_f. The *0* subscript designates the initial, inactivated configuration. Note that $l_{inactive}$ is a constant.

$$\begin{aligned} l_f &= l + l_{inactive} \\ l_{f,0} &= l_0 + l_{inactive} \end{aligned} \tag{20}$$

Strain ε is still computed relative to the McKibben fiber, so its definition is unchanged. Using the modified McKibben fiber force-strain relationship in equation (15), the pennate muscle force $F_{M,mod}$ is modeled as

$$F_{M,mod} = \kappa_F \pi r_0^2 P\left(a\left(1-\kappa_\varepsilon \varepsilon\right)^2 - b\right) n \cos\left(\theta\right) \tag{21}$$

If the load on the muscle is prescribed, the contraction of the muscle will depend on both its activation (pressure) and its configuration. Using equations (11) and (21), the pennate muscle stiffness is then

$$k_{M,mod} = \pi r_0^2 P \kappa_F n \left[\frac{2a\kappa_\varepsilon \left(1-\kappa_\varepsilon \varepsilon\right)}{l_0} \cos^2\left(\theta\right) + \frac{\left(a\left(1-\kappa_\varepsilon \varepsilon\right)^2 - b\right)}{l_f} \sin^2\left(\theta\right) \right] \tag{22}$$

To validate the model, a physical prototype of a pennate muscle is constructed as shown in Figure 7. The pennate muscle is composed of four fibers and has an adjustable thickness. The 3D printed fiber connections also act as turnbuckles for finely adjusting the initial fiber lengths. Data is collected on the

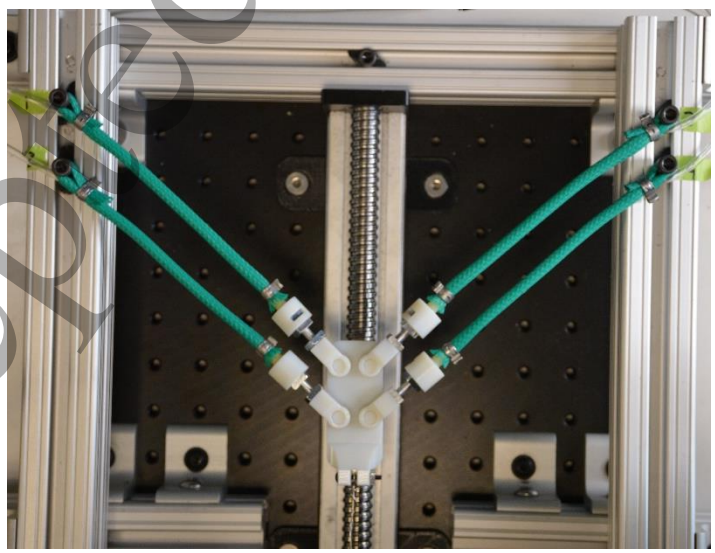

Figure 7: Overhead view of the physical pennate muscle prototype with four McKibben actuator fibers.

custom-built actuator testing platform introduced at the beginning of this section and described by Figure 4.

The geometry of the McKibben actuators used in the experiments is shown in Table 1. Four actuators are used to facilitate future inclusion of other bioinspired hierarchical behaviors, including orderly recruitment. Quasi-static force-strain data is collected for two thickness configurations at activation pressures of 207 kPa (30 PSI) and 276 kPa (40 PSI). Pressures greater than 276 kPa (40 PSI) saturated the load cell measurement range. All muscle fibers are at the same activation pressure during an experiment trial. Initial pennation angle is computed by digital measurement of an overhead photograph and validated using measured lengths and geometric relationships. Muscle force data are plotted with the muscle analytic model in Figure 8 for two configurations and two pressures. Figure 8a and Figure 8b show the force-contraction and stiffness-contraction models and data for an actuator thickness of t = 13 cm. Figure 8c and Figure 8d show the force-contraction and stiffness-contraction models and data for an actuator thickness of t = 15 cm. Data and models show good agreement, except for a noticeable deviation at zero-contraction for 207 kPa in Figure 8d. The large spike in the data is observable in the slope of the 207 kPa force data in Figure 8c. Because the pennate actuator model is constructed directly from the McKibben model, any parameter uncertainty and unmodeled effects in the McKibben model are propagated into the pennate actuator data. Note that for the pennate actuator model to represent the data well, the McKibben actuator must have an accurate model, because any modeling errors will be reflected n times in the pennate actuator model.

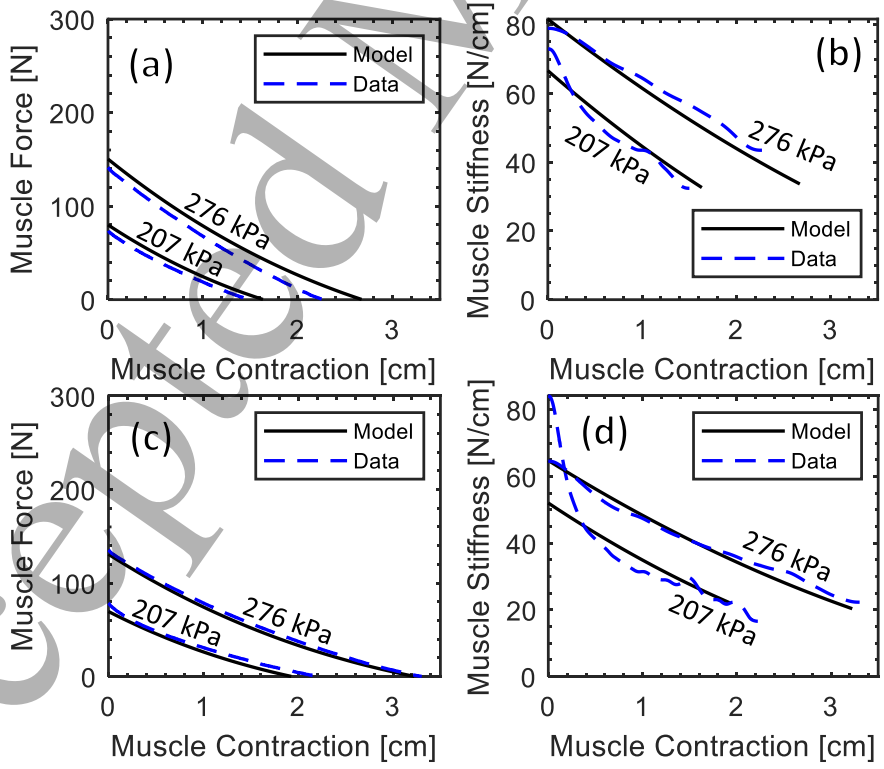

Figure 8: Force and stiffness vs contraction model and data for two pennate muscle configurations and two different pressures. (a) and (b) are for a thickness of 13 cm, (c) and (d) are for a thickness of 15 cm.

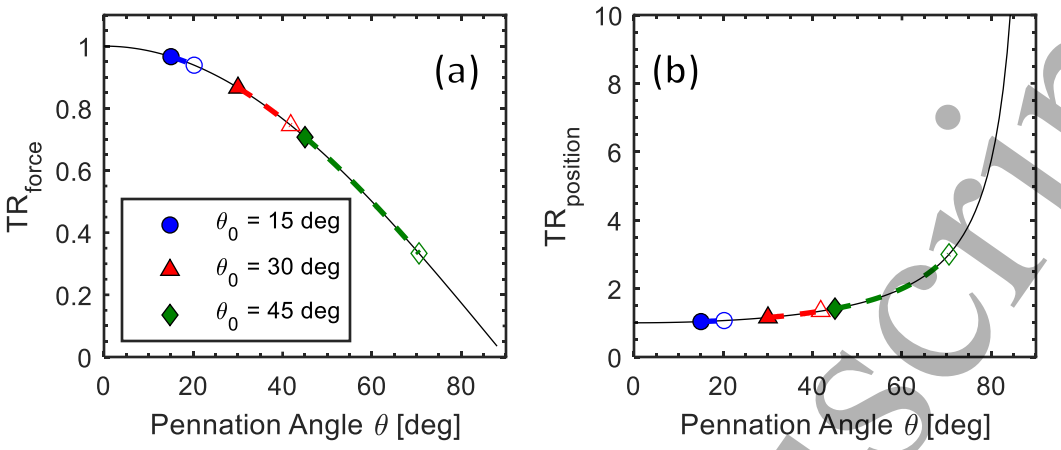

Figure 9: Plots showing (a) the force transmission ratio and (b) the position transmission ratio relating the pennate actuator and fiber actuator as a function of pennation angle. The filled markers indicate an initial configuration, and the empty makers indicate the configuration at 25% fiber strain. A more oblique pennate actuator will traverse a greater range of transmission ratios than a more-parallel pennate actuator.

Analysis – Using the McKibben model to understand the pennate actuator

Using the analytical model, detailed analysis can be performed to understand actuator performance via case studies. This section outlines the pennate actuator transmission ratio, blocked-force, free-strain, and a comparison between pennate actuator isotonic and isobaric contractions.

Transmission ratio

The muscle model shows that fiber force is attenuated by the cosine of the pennation angle, and a change in fiber displacement is amplified by the secant of the pennation angle. To understand the effects of pennate muscle configuration, the transmission ratios are plotted in Figure 9. For contractile fibers, the initial configuration of the actuator (parameterized by the initial pennation angle θ_0) and the maximum muscle strain dictate what portion of the transmission ratio curve the contraction will traverse. For example, a pennate muscle with unit fiber length, an initial pennation angle of 30 degrees, and fibers that contract 25% will have a maximum pennation angle of 42 degrees. Variations of this scenario are shown in Figure 9. For the aforementioned scenario (denoted by red triangles in Figure 9), the contraction has an initial force transmission ratio of 0.87, the point moves along the force transmission ratio curve as the actuator contracts, and has a final force transmission ratio of 0.75. Similarly, the position transmission ratio has an initial value of 1.16 and a final value of 1.34. Note that pennate actuators using the same fibers, but with different initial pennation angles, will travel different regimes of these curves. A more oblique pennate actuator will traverse a greater range of transmission ratios than a more-parallel pennate actuator.

Pennate actuator blocked-force

For a contractile pennate actuator at a constant pressure, the initial configuration represents the maximum force because it is the minimum pennation angle. Using this knowledge, the muscle blocked-force can be computed via equation (15), which represents the maximum force the pennate actuator can produce.

$$F_{m,blocked} = \kappa_F \pi r_0^2 P(a-b) n \cos(\theta_0)$$
$$\theta_0 = \sin^{-1}\left(\frac{t}{l_{f0}}\right) \quad (23)$$

At sufficiently high pressure (i.e., as κ_F approaches 1), the blocked-force increases linearly with pressure, just like with a McKibben fiber. To maximize the transmission of fiber force to muscle force, the pennation angle should be as small as possible, orienting the fibers more parallel.

Pennate actuator free-contraction

Pennate actuator free-contraction is the maximum contraction of the actuator under a zero-load condition. When considering a single McKibben actuator, the ideal fiber force equation has two scenarios for zero-force to occur: either the trivial case when the actuator is at zero pressure, or when $\varepsilon = \varepsilon_{free} = 1 - \sqrt{b/a}$. When considering the pennate actuator, a third zero exists when the pennation angle approaches a singularity configuration at θ = 90 degrees. Scenarios two and three need to be considered when analyzing the free-contraction of the pennate actuator.

To maximize free-contraction, the muscle thickness should equal the fiber free-length (plus any inactive length). This represents the fibers simultaneously approaching free-length as the muscle approaches its singularity. If the muscle thickness is smaller than the fiber free-length, the fiber will stop contracting

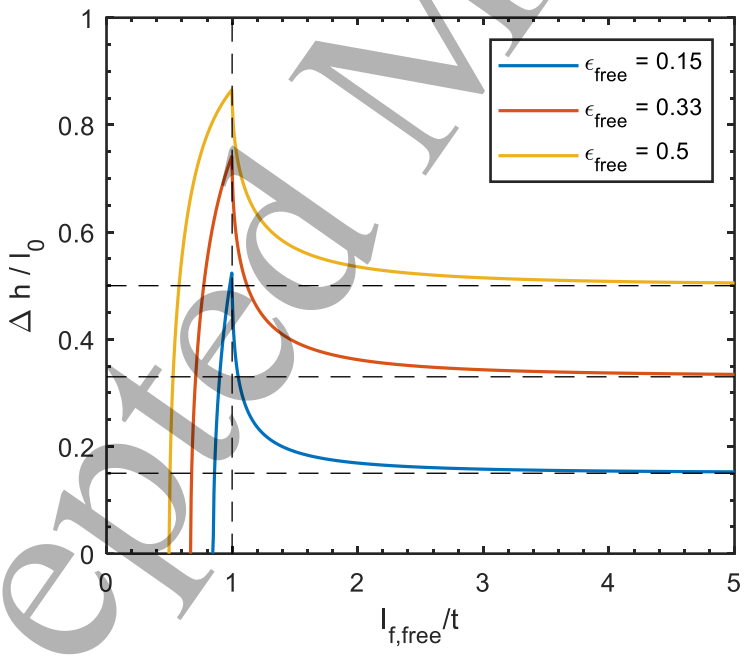

Figure 10: The relationship between pennate actuator stroke (non-dimensionalized by initial fiber length) and pennate actuator configuration (fiber free-length non-dimensionalized by pennate actuator thickness). The horizontal-axis value represents the fiber free-length divided by the constant muscle thickness, and the vertical-axis value represents the pennate actuator stroke. Pennate actuator free contraction is maximized when the thickness is equal to the fiber free length.

before the fibers have completely rotated, and muscle free-contraction will not be maximized. This scenario is represented in Figure 10 by the curves on the right-hand side of the vertical dashed line. Figure

10 shows the muscle contraction (non-dimensionalized by the initial fiber length) as a function of the ratio of fiber free-length to muscle thickness. If the muscle thickness is larger than the free-length of the muscle, the fibers will completely rotate before they are fully contracted, resulting in a free-contraction that is not maximized. This scenario is represented in Figure 10 by the curves on the left-hand side of the vertical dashed line. The nondimensional free-contraction $\Delta h/l_0$ is represented by the piecewise function

$$\begin{aligned} \frac{\Delta h}{l_0} &= \cot\left(\theta_0\right) - \cot\left(\theta_{free}\right) \quad & \frac{l_{f,free}}{t} \le 1 \\ \frac{\Delta h}{l_0} &= \cot\left(\theta_0\right) & \frac{l_{f,free}}{t} > 1 \end{aligned} \tag{24}$$

and $l_{f,free} = l_{inactive} + l_0\left(1-\varepsilon_{free}\right)$, where $\varepsilon_{free} = 1-\sqrt{b/a}$ in the ideal case, or equal to the polynomial determined in equation (19) when considering material effects. θ_{free} is the pennation angle at the free-contraction,

$$\theta_{free} = \sin^{-1}\left(\frac{t}{l_{f,free}}\right) \tag{25}$$

When fiber free-length equals the muscle thickness (i.e., $l_{f,free}/t = 1$), the muscle contraction is maximized, as denoted by the peaks of the curves. The corresponding pennation angle is denoted as θ_0^*. When the fiber free-length is greater than the thickness (i.e., a more "parallel" configuration), the non-dimensional muscle contraction asymptotically approaches a value equal to the fiber free-strain. This is because the fibers rotate less in a more-parallel configuration, meaning the muscle contraction is nearly equivalent to the fiber contraction. When the fiber free-length is smaller than the thickness, the fibers do not fully contract before the fiber rotation is maximized, limiting contraction. Horizontal intercepts of the plot denote the maximum muscle thickness, where $t = l_0$ in the extreme case. The vertical axis of the curve represents the stroke amplification effect of the pennate muscle. For example when $\varepsilon_{free} = 0.33$, the maximum $\Delta h/l_0$ value is 0.74. This means that the fiber has contracted 33% of its initial length, but the muscle stroke is 74% of the fiber's initial length. When $\Delta h/l_0 > \varepsilon_{free}$, the pennate actuator maximum contraction is greater than the fiber maximum contraction. Note that Figure 10 is general for any pennate actuator, regardless of its constituent fiber actuators.

At play here is the idea of work performed by the fiber and muscle. When $l_{f,free}/t$ is less than 1, the fibers cannot fully contract, meaning less work is performed than an actuator with the same length fibers but less thickness. When $l_{f,free}/t$ is greater than or equal to 1, the output work of the muscle (divided by the number of fibers) equals the work done by each fiber. As long as the fibers can fully contract, all configurations produce the same amount of work, shown in equation (26). The transmission ratio effect of the pennate actuator serves to alter this work from high force, low stroke to lower force, with increased contraction.

$$W = n\int_{l_0}^{l_{f,free}} F_f\,dl = \int_{h_0}^{h} F_m\,dh \tag{26}$$

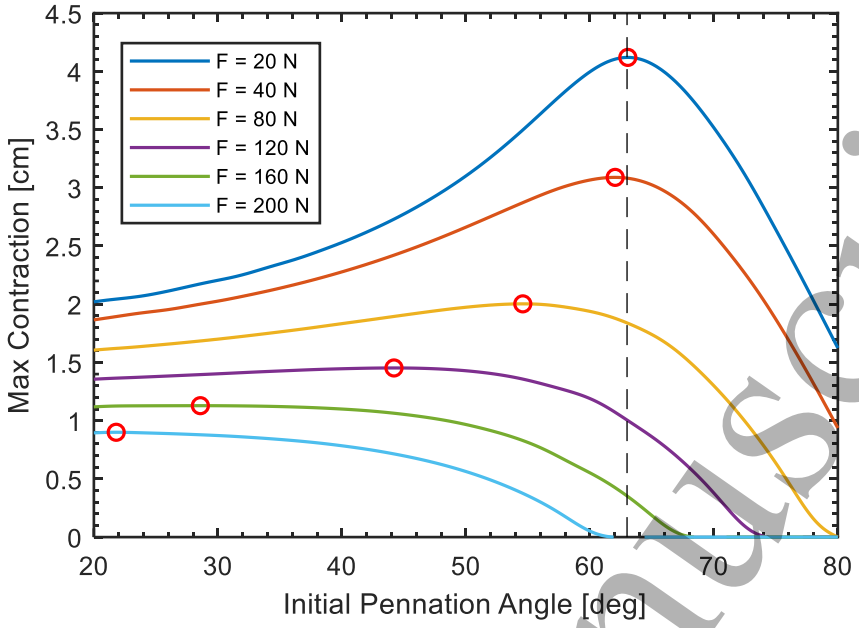

Figure 11: Maximum contractions vs initial pennation angle for six different isotonic loads. The red circles denote the maximum of each curve. The vertical dashed line represents the configuration when $t = l_{f,free}$, i.e. $\theta_0 = \theta_0^*$. The applied pressure is bounded at 414 kPa (60 PSI). The simulations use McKibben actuator parameters from Table 1 and Table 2. As the load increases, the configuration maximizing contraction trends towards a more parallel alignment.

Isotonic contractions

Due to the transmission ratio effect of the pennate geometry, pennate actuators with identical fibers but different initial pennation angles will have different contraction behaviors. This is especially evident during loaded contractions, where highly pennate actuators will not be able to effectively move large loads. To explore this effect, isotonic contractions are modeled by implicitly computing the pressure required to create a constant force at a given position. To maintain continuity with the previous experiments, pressure is bounded to a maximum of 414 kPa (60 PSI). Figure 11 summarizes this by displaying the maximum contraction as a function of initial configuration for six constant loads. For small loads, the maximum contraction occurs when the initial pennation angle is close to θ_0^*. As the load increases, the configuration maximizing contraction trends towards a more parallel alignment. When the load is sufficiently high, some highly pennate configurations are unable to generate any contraction. Future work should explore methods of adapting the pennate actuator's configuration in response to changing contraction and force demands.

Stiffness during isobaric and isotonic contractions

We have previously shown that stiffness increases with pressure and a more parallel configuration. Alternatively, reducing pressure or increasing the pennation angle serves to reduce the stiffness of the actuator. However, if the muscle contracts isotonically, the required input pressure will increase (effectively increasing stiffness) and the pennation angle will increase (effectively reducing stiffness). To more clearly pose these competing effects, consider two configurations of the same pennate actuator. For configuration 1, consider a pennation angle θ_1, force F_1, pressure P_1 required to produce F_1, and stiffness k_1. For configuration 2, consider a pennation angle $\theta_2 > \theta_1$, an identical force $F_2 = F_1 = F$, a pressure $P_2 > P_1$ required to produce F, and a stiffness k_2. It is unclear whether k_1 is less or greater than k_2.

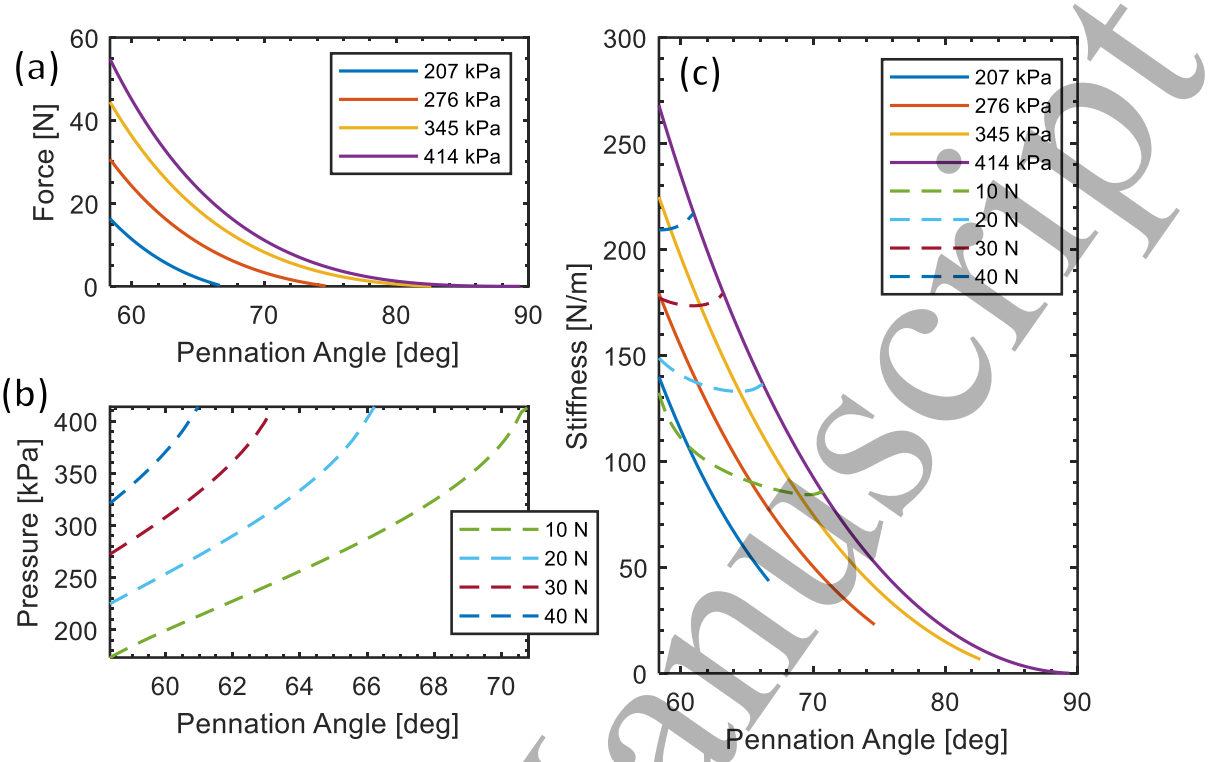

Figure 12: (a) Force vs pennation angle for isobaric contractions, (b) required input pressure vs pennation angle for isotonic contractions, and (c) stiffness vs pennation angle for isobaric and isotonic contractions. Given a desired position and load, the required pressure and stiffness can be computed.

Considering a case study where muscle thickness equals the fiber free-length at 414 kPa (60 PSI), isotonic contractions of the McKibben pennate actuator are explored. Figure 12a shows muscle force as a function of pennation angle when undergoing isobaric quasi-static contractions. Figure 12b shows the required input pressure to create an isotonic contraction as a function of pennation angle. Note that Figure 12b's vertical axis is limited to 414 kPa (60 PSI) because the correction factors κ_F and κ_ε considered here are valid from 138-414 kPa (20-60 PSI). Figure 12c combines this information, showing the muscle stiffness for isotonic and isobaric contractions as a function of pennation angle. Figure 12c shows that there is a nonlinear relationship governing stiffness change as a McKibben pennate actuator contracts isotonically. If a 10N isotonic contraction is considered, the changing pennation angle reduces stiffness at a higher rate than the increasing pressure serves to stiffen the actuator. Therefore, at the fully contracted position, the muscle is less stiff than at the uncontracted position. The opposite is true as the isotonic force is increased – at a 40N isotonic contraction, the actuator stiffness is greatest when it is fully contracted because the increased pressure stiffens the muscle more quickly than the fiber rotation decreases stiffness.

For a specific application when parameters such as fiber length are known, the contraction can be solved computationally. If thickness is constant, the equilibrium position and pressure are unique. However, if thickness can be varied, the extra control will allow both force and stiffness to be prescribed within a bounded range, which is outside the scope of this paper. This work lays the foundation for extension into a true variable stiffness actuator.

Conclusion

This paper outlines the conceptualization, design, modeling, and analysis of a bio-inspired pennate actuator. The pennate actuator is one embodiment of a hierarchical actuator, which generally offer the ability to use geometric complexity to tailor configuration, speed, force, efficiency, stroke, or redundancy. To this end, a constitutive kinematic model relating the muscle-level force and strain to the fiber-level force and strain was first developed. The kinematic model is used to describe the transmission ratio, which describes the relationship between the muscle outputs and the fiber inputs as a function of pennation angle. A model for the muscle stiffness was also developed using the kinematic relationships, and the actuator was shown to have a position-dependent stiffness. To validate the kinematic model, a proof-of-concept physical model of a pennate muscle was built; this prototype showed nonlinear stiffness as a function of position as predicted by the model, even though linear stiffness fibers were used. Next, a pennate muscle with McKibben actuators was built. By adapting existing McKibben models to the new model in this paper, the McKibben pennate actuator model was validated against experimental data. Data was collected using a custom built actuator testing platform. The testbed is capable of controlling actuator pressure in closed loop, prescribing position, measuring force, and reconfiguring to test a variety of pennate muscle configurations. After validation, the model was used to further analyze the actuator characteristics. Relationships between the configuration and gear ratio were then outlined. The couplings between free-contraction, blocked-force, and loaded contractions to initial configuration were analyzed. Finally, relationships between stiffness and configuration were better understood by examining the actuator model in isobaric and isotonic contractions. This work lays the foundation for the creation of a versatile, adaptive pennate actuator. Advanced actuation techniques are needed to continue making improvements in the safety, efficiency, and performance of mobile robotics. To progress towards a functioning adaptive pennate actuator capable of altering configuration to meet force, stroke, and stiffness demands, future work should address the sensitivity of the pennate actuator to fiber parameter uncertainty and the implications of adjusting the number of constitutive actuators.

Acknowledgements

This material is based upon work supported by the National Science Foundation under Grant No. CMMI-1845203.

References

[1] Ueda J, Schultz J and Asada H 2017 *Cellular Actuators: Modularity and Variability in Muscle-inspired Actuation* (Butterworth-Heinemann)

[2] Huston D, Esser B, Spencer G, Burns D and Kahn E 2005 Hierarchical actuator systems *Smart Struct. Mater. 2005 Ind. Commer. Appl. Smart Struct. Technol.* **5762** 311

[3] Mathijssen G, Lefeber D and Vanderborght B 2015 Variable recruitment of parallel elastic elements: Series-parallel elastic actuators (SPEA) with dephased mutilated gears *IEEE/ASME Trans. Mechatronics* **20** 594–602

[4] Bryant M, Meller M A and Garcia E 2014 Variable recruitment fluidic artificial muscles: Modeling and experiments *Smart Mater. Struct.* **23**

[5] Kuo A 2007 Choosing Your Steps Carefully: Trade-offs between economy and versatility in dynamic walking bipedal robots *IEEE Robot. Autom. Mag.* **14** 18–29

[6] Jenkins T E, Chapman E M and Bryant M 2016 Bio-inspired online variable recruitment control of fluidic arti ficial muscles *Smart Mater. Struct.* **25** 125016

[7] Jenkins T E and Bryant M 2019 Variable stiffness soft robotics using pennate muscle architecture **1096505** 4

[8] Azizi E, Brainerd E L and Roberts T J 2008 Variable gearing in pennate muscles *Proc. Natl. Acad. Sci.* **105** 1745–50

[9] Holt N C, Danos N, Roberts T J and Azizi E 2016 Stuck in gear: age-related loss of variable gearing in skeletal muscle *J. Exp. Biol.* **219** 998–1003

[10] Azizi E and Roberts T J 2014 Geared up to stretch: pennate muscle behavior during active lengthening *J. Exp. Biol.* **217** 376–81

[11] Azizi E and Roberts T J 2013 Variable gearing in a biologically inspired pneumatic actuator array *Bioinspir. Biomim.* **8** 026002

[12] Kianzad S, Pandit M, Lewis J D, Berlingeri A R, Haebler K J and Madden J D W 2015 Variable stiffness structure using nylon actuators arranged in a pennate muscle configuration 94301Z

[13] Pratt G A and Williamson M M 1995 Series elastic actuators *Proceedings 1995 IEEE/RSJ International Conference on Intelligent Robots and Systems. Human Robot Interaction and Cooperative Robots* vol 1 (IEEE Comput. Soc. Press) pp 399–406

[14] Vanderborght B, Albu-Schaeffer A, Bicchi A, Burdet E, Caldwell D G, Carloni R, Catalano M, Eiberger O, Friedl W, Ganesh G, Garabini M, Grebenstein M, Grioli G, Haddadin S, Hoppner H, Jafari A, Laffranchi M, Lefeber D, Petit F, Stramigioli S, Tsagarakis N, Van Damme M, Van Ham R, Visser L C and Wolf S 2013 Variable impedance actuators: A review *Rob. Auton. Syst.* **61** 1601–14

[15] Wolf S, Grioli G, Eiberger O, Friedl W, Grebenstein M, Hoppner H, Burdet E, Caldwell D G, Carloni R, Catalano M G, Lefeber D, Stramigioli S, Tsagarakis N, Van Damme M, Van Ham R, Vanderborght B, Visser L C, Bicchi A and Albu-Schaffer A 2016 Variable Stiffness Actuators: Review on Design and Components *IEEE/ASME Trans. Mechatronics* **21** 2418–30

[16] Tonietti G, Schiavi R and Bicchi A Design and Control of a Variable Stiffness Actuator for Safe and Fast Physical Human/Robot Interaction *Proceedings of the 2005 IEEE International Conference on Robotics and Automation* (IEEE) pp 526–31

[17] Kardel T 1990 Niels Stensen's geometrical theory of muscle contraction (1667): A reappraisal *J. Biomech.*

[18] Otten E 1988 Concepts and models of functional architecture in skeletal muscle *Exerc. Sport Sci. Rev.*

[19] Benninghoff A and Rollhäuser H 1952 Zur inneren Mechanik des gefiederten Muskels *Pflugers Arch. Gesamte Physiol. Menschen Tiere*

[20] Wolf S, Grioli G, Eiberger O, Friedl W, Grebenstein M, Hoppner H, Burdet E, Caldwell D G, Carloni R, Catalano M G, Lefeber D, Stramigioli S, Tsagarakis N, Van Damme M, Van Ham R, Vanderborght B, Visser L C, Bicchi A and Albu-Schaffer A 2016 Variable Stiffness Actuators: Review on Design and Components *IEEE/ASME Trans. Mechatronics* **21** 2418–30

[21] Savitzky A and Golay M J E 1964 Smoothing and Differentiation of Data by Simplified Least Squares

Procedures *Anal. Chem.*

[22] Meller M, Chipka J, Volkov A, Bryant M and Garcia E 2016 Improving actuation efficiency through variable recruitment hydraulic McKibben muscles: modeling, orderly recruitment control, and experiments *Bioinspir. Biomim.* **11** 065004

[23] DeLaHunt S A, Pillsbury T E and Wereley N M 2016 Variable recruitment in bundles of miniature pneumatic artificial muscles *Bioinspir. Biomim.* **11** 056014

[24] Tondu B and Lopez P 2000 Modeling and control of McKibben artificial muscle robot actuators *IEEE Control Syst. Mag.* **20** 15–38

[25] Ching-Ping Chou and Hannaford B 1996 Measurement and modeling of McKibben pneumatic artificial muscles *IEEE Trans. Robot. Autom.* **12** 90–102

[26] Meller M A, Bryant M and Garcia E 2014 Reconsidering the McKibben muscle: Energetics, operating fluid, and bladder material *J. Intell. Mater. Syst. Struct.* **25** 2276–93

[27] Chapman E, Jenkins T and Bryant M 2016 Parametric study of a fluidic artificial muscle actuated electrohydraulic system *ASME 2016 Conference on Smart Materials, Adaptive Structures and Intelligent Systems, SMASIS 2016* vol 2